Empirical Analysis of Surface Subsidence Associated with Caving

Resolution Copper Mine Plan of Operations

ITASCA
Consulting Group, Inc.

Empirical Analysis of Surface Subsidence Associated with Caving
Resolution Copper Mine Plan of Operations

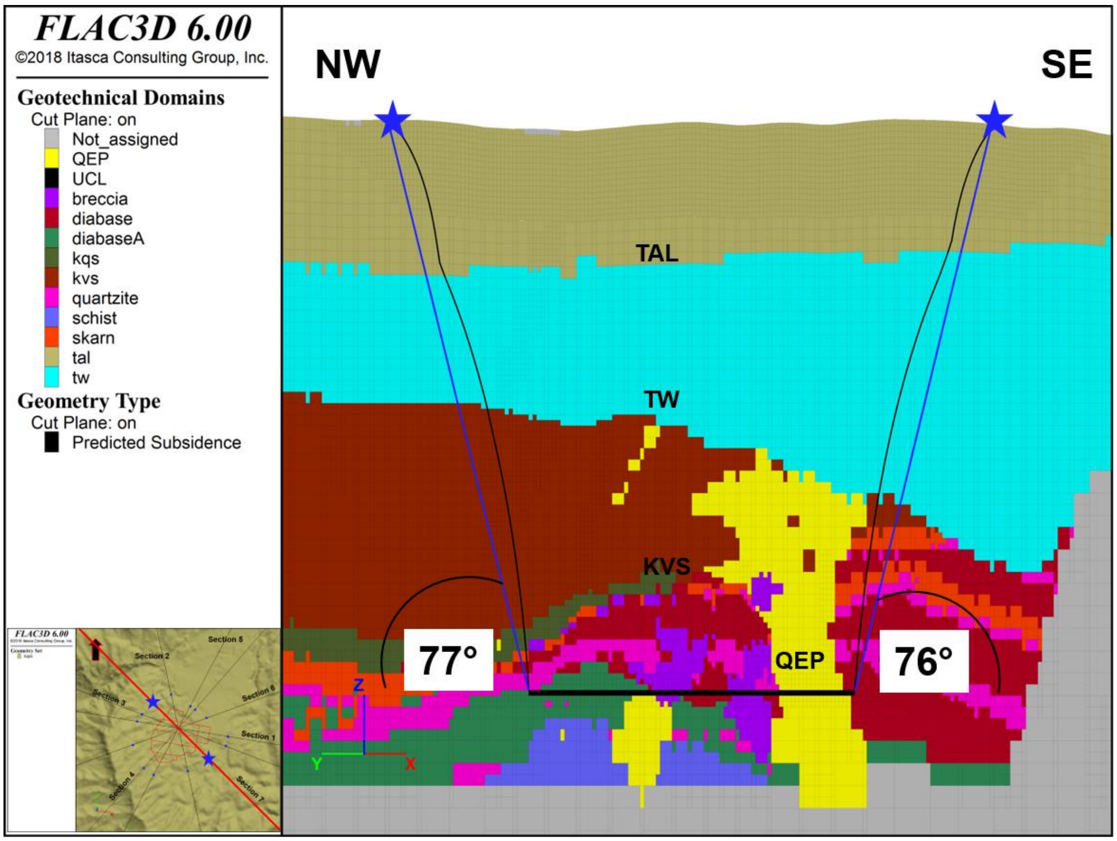

May 16, 2019
2-4208-04:19R32

Prepared For:
Resolution Copper Mining LLC
Prepared By:
Christian Cancino,
Tryana Garza-Cruz,
Itasca Consulting Group, Inc
Matthew Pierce,
Pierce Engineering

ITASCA
Consulting Group, Inc.

111 Third Ave South, Suite 450
Minneapolis, MN 55401
phone: 1 612 371-4711 fax: 1 612 371-4711
email: icg@itascacg.com
web: www.itascacg.com

Executive Summary

This report summarizes the results of an updated empirical prediction of subsidence performed by Itasca Consulting Group, Inc. (Itasca) for Resolution Copper Mining, LLC (Resolution Copper).

This study evaluates the subsidence associated with caving at Resolution Copper through estimation of the angle of break using the empirical method developed by Laubscher (2000).

A probabilistic approach of Laubscher's Method has been carried out using Monte Carlo simulations to estimate a distribution of angle of break over seven sections studied. The In Situ Rock Mass Rating (IRMR) distributions per geotechnical domain are used as input for random sampling in the Monte Carlo simulations. A Mining Rock Mass Rating (MRMR) adjustment procedure was carried out comparing the global rock mass strength to the mining-induced hoop stresses around the cave given by the Kirsch analytical solution.

The results indicate an average angle of break of 77 degrees, which is in general agreement with the results of previous numerical modeling analysis predicting cave angles between 70 – 78° (Garza-Cruz & Pierce, 2017).

Although Laubscher's empirical method is based on limited data, it is a useful approach to capture tendencies and to obtain an initial understanding of subsidence in the mine.

Table of Contents

1.0 INTRODUCTION

Block caving is increasingly favored as a mining method for large, lower grade ore bodies, especially as companies target deeper resources or transition underground from open pits that have reached the end of their mine life. As a mass mining method, block caving can result in ground collapse and surface deformations. Of concern is mine infrastructure located on surface or the impact that ground deformations may have on areas surrounding the mine.

Empirical databases provide a means to learn from case histories, discover causal relationships between different contributing factors, establish guidelines for design, and to help provide a starting point to undertake more sophisticated analysis (e.g. three-dimensional non-linear numerical modeling). One of the most commonly cited is Laubscher's method (Laubscher, 2000).

This report outlines an updated empirical estimation of subsidence resulting from caving at Resolution Copper. The estimation uses Laubscher's method with the IRMR database collected on the Resolution Copper deposit.

2.0 BACKGROUND

2.1 Geotechnical Properties

2.1.1 Geology

The geology at Resolution is complex, with many rock types present in the lithological column. The geological interpretation used in this study was provided by Resolution Copper as a series of DXF wireframes with associated hierarchy, as some of these wireframes overlapped. These DXFs were used to define the spatial distribution of the different geological units, as shown in Figure 1 and Figure 2. The production level is at an elevation of -2540 ft below MSL, approximately 2050 m below surface on average.

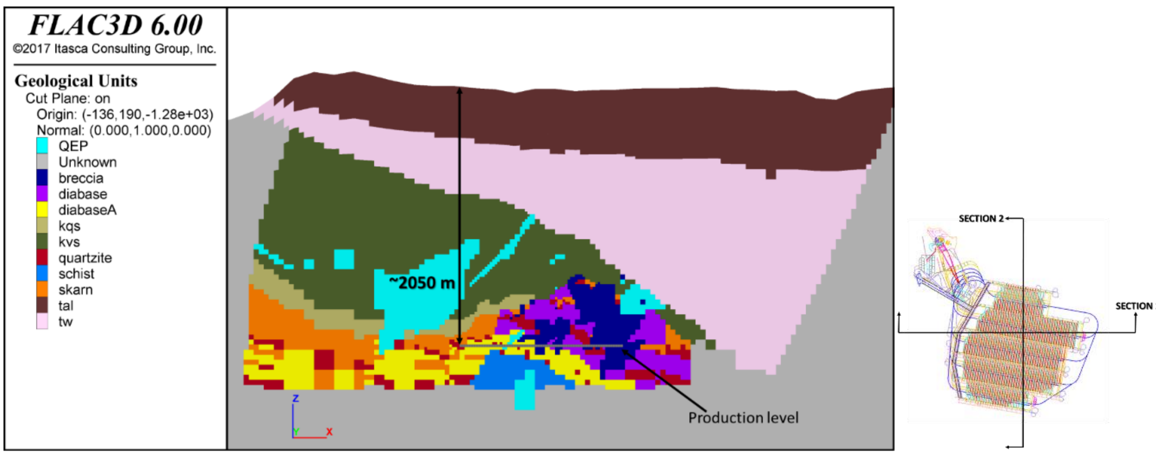

Figure 1 Spatial distribution of lithology on an East-West cross-section looking north.

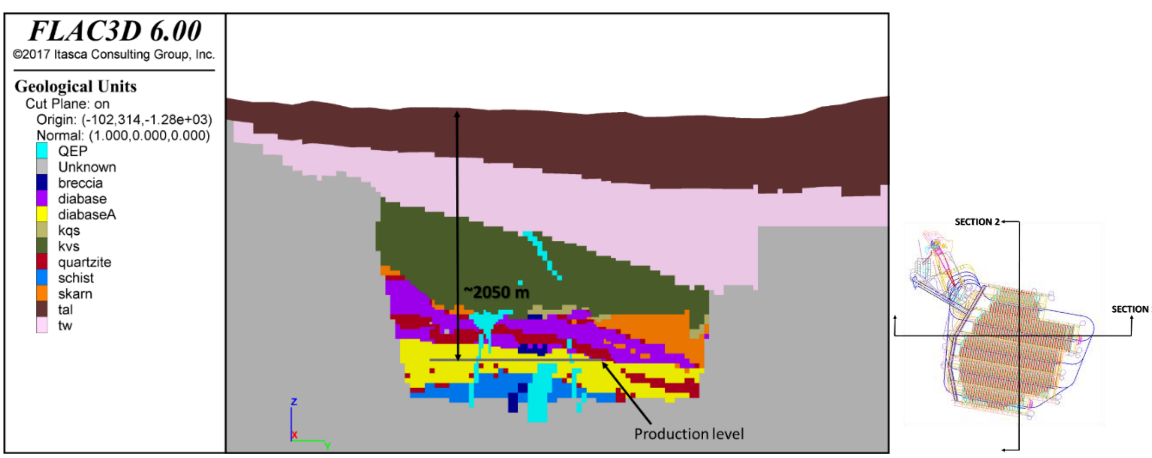

Figure 2 Spatial distribution of lithology on North-South cross-section looking west.

2.1.2 In Situ Rock Mass Rating (IRMR)

Resolution Copper provided the IRMR values for each geotechnical domain. They are presented in Figure 3 and Table 1. These distributions form the basis of the probabilistic analysis reported here.

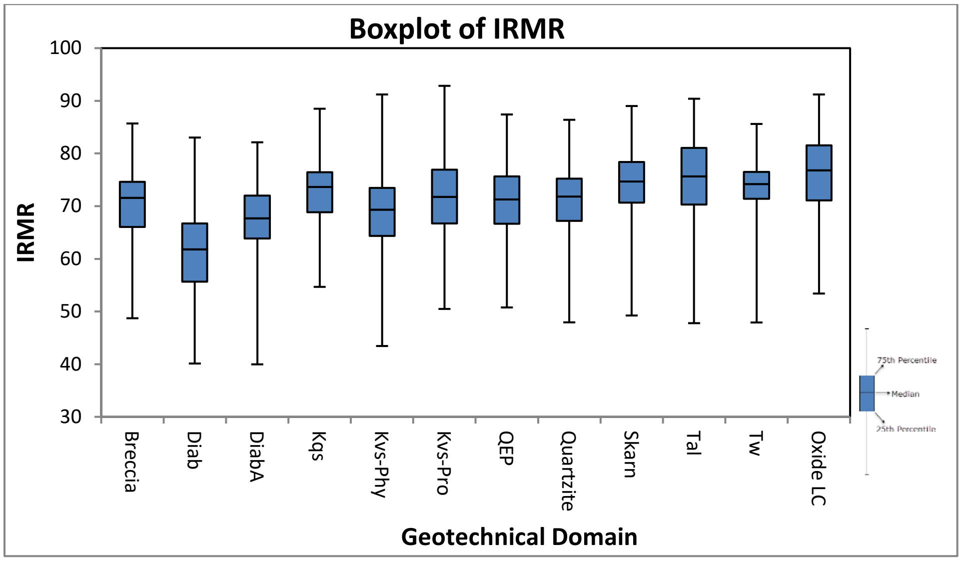

Figure 3 Distribution of IRMR values for each geotechnical domain.

Table 1 IRMR Data for Each Geotechnical Domain Used in This Study

	IRMR Data			
Unit	P50	SD	Min Value	Max Value
Quartzite	71	6	48	86
Diabase with anhydrite	67	8	40	82
Diabase	61	8	40	83
Skarn	74	6	49	89
KQS	73	6	55	88
KVS-Phy	69	7	43	93
QEP	71	6	51	87
Breccia	70	6	49	86
Tw (Whitetail)	73	6	48	86
Tal (Apache Leap Tuff)	75	8	48	90

2.1.3 Rock Mass Strength

The rock mass properties for the different geological units were provided by Resolution Copper.

Table 2 lists the rock mass parameters of the geological units used in this study to do a relative comparison to the likely induced stresses as a result of mining, which is used to inform the mining induced stress adjustment in the conversion of IRMR to MRMR. These rock mass properties have been used in previous numerical analyses of subsidence carried out by Itasca (Garza-Cruz & Pierce, 2017).

Table 2 Data and Estimated Hoek-Brown Parameters by Geologic Unit

	Data				Hoek Brown Parameters			
					Peak Strength			Global Rock Mass Strength
Unit	GSI	σ_d (MPa)	m_d	Density (kg/m^3)	m_{rm}	s	a	σ_{cm} (MPa)
Diabase, Basalt	54	54	12	2600	2.3	0.006	0.5	11
Diabase with anhydrite	62	106	15	2600	3.9	0.0147	0.5	29
Breccia, QEP	54	55	15	2600	2.9	0.006	0.5	13
Quartzite	69	103	21	2600	6.9	0.0319	0.5	38
Tal (Apache Leap Tuff)	64	66	30	2600	8.3	0.0183	0.5	26
Tw (Whitetail)	73	23	22	2600	8.4	0.0498	0.5	10
KVS, KQS	66	46	30	2600	8.9	0.0229	0.5	19
Skarn	63	59	22	2600	5.9	0.0164	0.5	20

2.2 Mine Design

Resolution Copper proposes to mine the orebody via panel caving. The extraction level would be located at 2540 ft below MSL (a depth of approximately 2050 m below ground surface). The design used in this analysis is shown in Figure 4.

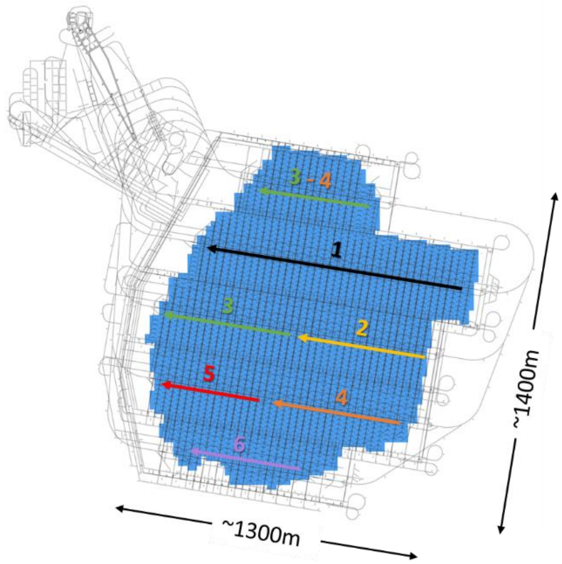

Figure 4 Proposed Layout

2.3 In Situ Stress

The in-situ stress regime used for the analysis presented here was provided by Resolution Copper and is based upon hydrofracturing tests done on site.

- The maximum principal stress, σ_1, is the vertical stress and is equal to the overburden.
- The intermediate principal stress, σ_2, is oriented in a north-south direction and has a magnitude of 80% of σ_1.
- The minimum principal stress, σ_3, is oriented in the east-west direction and has a magnitude of 50% of σ_1.

Table 3 lists stress field magnitude, which is also seen in Figure 5.

Table 3 In situ stress field used.

Principal Stress	Magnitude
$\boldsymbol{\sigma_V}$	25.5*z [km]
$\boldsymbol{\sigma_H}$	20.4*z [km]
$\boldsymbol{\sigma_h}$	12.75*z [km]

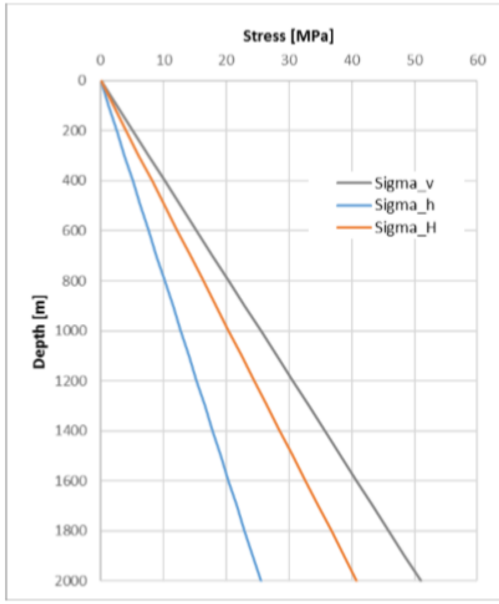

Figure 5 In situ stress regime used in the analysis.

3.0 LAUBSCHER'S EMPIRICAL METHOD

An empirical approach to predicting surface subsidence limits due to caving operations was developed by Laubscher (2000). The method is based on Laubscher's MRMR (Mining Rock Mass Rating) classification system. It relates the predicted cave angle to the MRMR, mining depth, and drawdown of the material being caved. Therefore, thorough knowledge of the various lithological and geotechnical units that the cave will propagate through is important. The method is founded on the premise that the stronger the rock mass (high MRMR), the steeper the cave angle. In addition, the broken material within the muck pile is assumed to offer confining support to the cave walls. Other controlling parameters, such as stress and structure, are accounted for in the derivation of the MRMR. Laubscher's method is the most commonly used empirical method for estimating subsidence in caving operations.

After defining the various geotechnical units in which the cave will propagate, the MRMR for each unit is determined. A cave material factor for each unit is then required using the following:

$$Factor_{caved\ material} = \frac{density\ of\ caved\ material}{1.5} * \frac{height\ of\ caved\ material}{100} * \frac{depth\ below\ surface}{minimum\ span}$$

With this factor and the MRMR for each unit, the cave angle can be then determined from the chart in Figure 6.

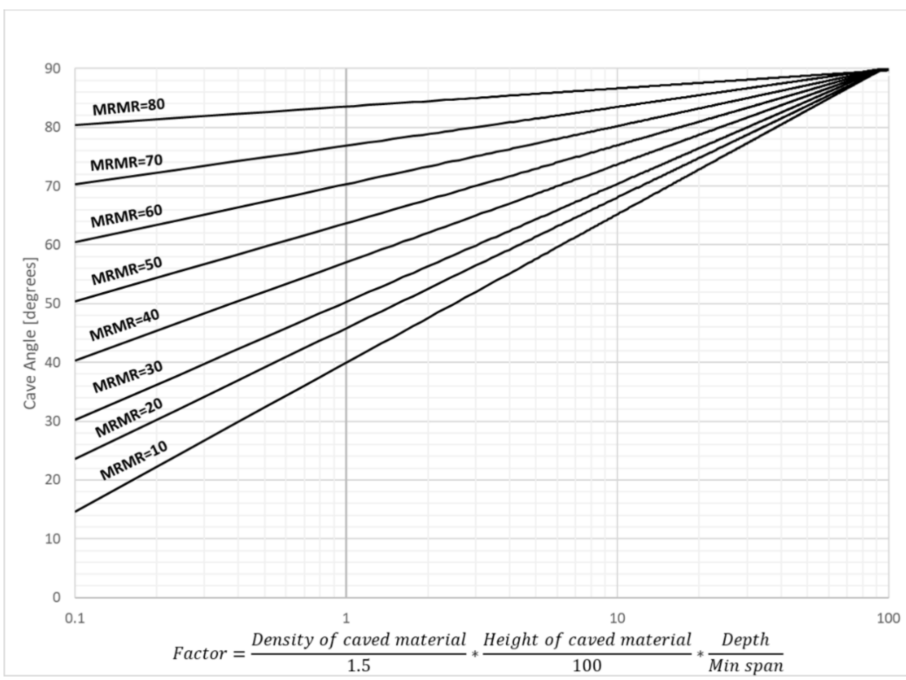

Figure 6 Laubscher's empirical design chart for assessing cave angle (angle of break) as a function of mining rock mass rating (MRMR) value and the height and depth of the caved block.

When a cave breaches the surface on the side of a hill or mountain, toppling of the upper slopes often occurs. In a similar manner, if an open pit has changed over to a caving operation, once the cave back begins to interact with the toe of the pit slope, slope failures will be noted. Large-scale structures will also modify the break back, with daylighting structures increasing the break back and non-daylighting, steeply dipping structures reducing it.

The application of Laubscher's method requires sound engineering judgment and a full consideration of the geological and geotechnical setting in which it is being applied.

The cave angle (or angle of break) referred to by Laubscher is defined by van As et al. (2003) as the angle of the line extending from the edge of the extraction level to the edge of the zone of active caving, as seen in Figure 7. The caved zone is usually located directly above the undercut footprint and thus is characterized as having the greatest surface disturbance, usually manifested as a crater filled with broken irregular blocks. van As et al. (2003) also define two further subsidence zones and corresponding angles: the fracture initiation angle is the angle measured from horizontal of the line extending from the edge of the extraction level to the edge of the zone of fracture (or zone of active movement). This zone encompasses all obvious surface deformations adjacent to the caved zone, typically characterized by large radial cracks and rotated and toppling blocks. The angle of subsidence marks the outermost zone and the limits of measurable surface deformations on surface. These are generally described as elastic or continuous non-elastic strains, with vertical displacements greater than 2 mm.

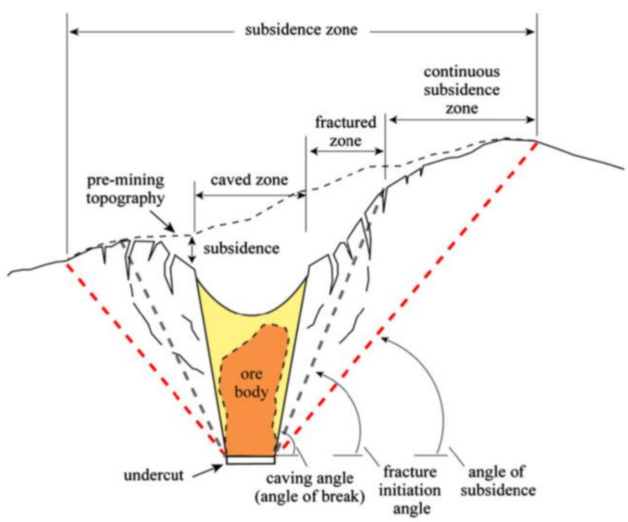

Figure 7 Definition of block caving deformation zones as defined by Van As et al. (2003).

4.0 PROBABILISTIC ANALYSIS OF LAUBCHER'S METHOD

Seven sections have been selected to estimate the subsidence at Resolution Copper, shown in Figure 8.

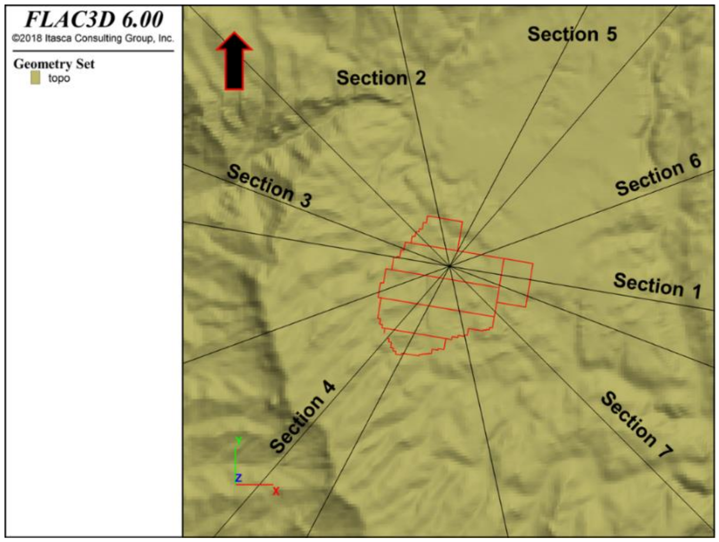

Figure 8 Sections of analysis (top view).

Due to the variability in geo-materials, a probabilistic analysis of Laubscher's method is carried out that involves randomly sampling an IRMR value from the associated distribution of the different geological units using @RISK. @RISK is an add-in to Microsoft Excel that facilitates risk analysis using Monte Carlo simulation.

Each examined cross-section is vertically subdivided into 10m layers. The methodology consists of sampling an IRMR value from the distribution of the geotechnical unit associated to each of the 10m layers in the section under study. Then an MRMR adjustment procedure is performed (detailed in the next section) for each subdivision (10 m height). This MRMR value is used in Laubscher's Method to estimate the angle of break for each subdivision and, lastly, to calculate the angle of break considering the minimum and maximum span and total depth. A total of 10,000 iterations were simulated, resulting in 10,000 computed cave angles.

Figure 9 shows a flowchart summarizing the methodology.

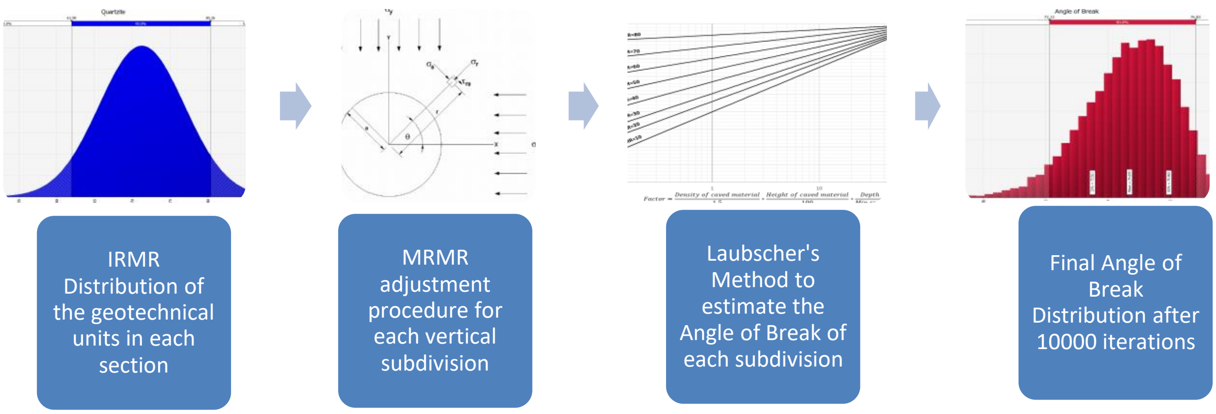

Figure 9 Flowchart of the methodology.

Two analyses were carried out per cross-section analyzed (one at each end of the UCL), resulting in two cave angle distributions per section due the differences in geology at each end of the UCL (14 cave angle distributions total).

4.1 Assumptions

a. IRMR is sampled as a random variable by assuming a normal distribution per geological domain.

b. An MRMR adjustment procedure is carried out for the resulting IRMR value, per iteration.

c. Ten thousand iterations are run for each simulation.

d. Height of caved material will be the same as depth to calculate the caved material factor in Laubscher's Method.

e. The density of caved material is estimated by using an average bulking factor of 0.14 (Garza-Cruz & Pierce, 2017), which gives a density of 2290 kg/m^3.

f. The distance between the UCL and the surface has been divided into 10 m high layers, with an MRMR characterization and associated break angle calculation per layer. The span from the underlying layer is used for the break angle calculation in the current layer

g. The topography at Resolution is considered flat for the calculation of break angle.

h. The angle of break is calculated by considering the minimum and maximum span and the total depth (distance between surface and undercut level).

4.2 Mining Rock Mass Ratio Adjustment Procedure

Following the guidelines given by Laubscher & Jakubec (2001) the IRMR value sampled from the input distribution is multiplied by an adjustment factor to give the MRMR rating (MRMR = adjustment factor * IRMR). This factor is a combination of several different adjustments:

- Weathering
- Joint-Orientation Adjustment
- Mining-Induced Stresses
- Blasting
- Water/Ice Adjustment

The cited authors consider that the MRMR for a caveability assessment would not have blasting as an adjustment, nor would it have weathering unless the weathering affects were so rapid as to exceed the rate of propagation resulting from structural and stress effects. The joint-orientation and mining-induced stress adjustments tend to complement each other. The purpose of the adjustment is for the geologist, rock mechanics engineer, and planning engineer to adjust the IRMR so that the MRMR is a realistic number that reflects the Rock Mass Rating (RMR) for that particular mining situation.

In this study, the weathering, blasting, and water effects were not considered, in accordance with the guidelines of Laubscher & Jakubec (2001). A joint orientation adjustment was not made since the rock mass is considered to be isotropic (i.e. no dominant joint orientation controlling stability).

Laubscher & Jakubec (2001) suggest that mining-induced stresses would contribute to the MRMR adjustment (between 120% and 60%), but do not provide explicit guidelines for its calculation. As a first approximation, the Kirsch analytical solution for stresses around a circular hole in an elastic plate was used to estimate the mining-induced hoop stress in the cave boundary, σ_θ, at a given depth by assuming a cylindrical cave shape. This analytical solution is schematized in Figure 10.

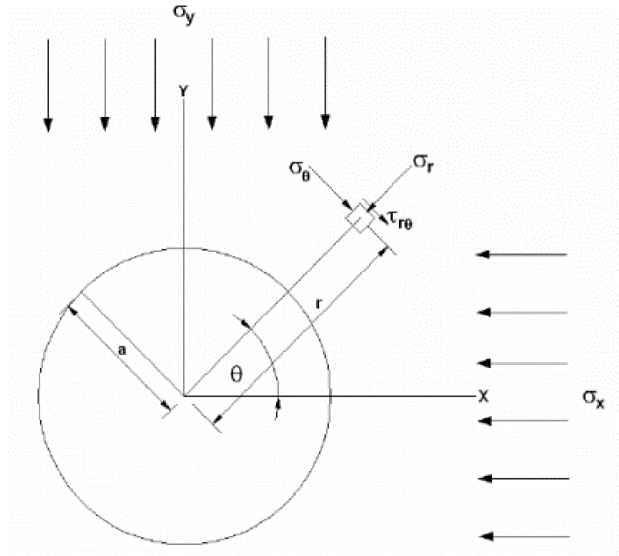

Figure 10 Kirsch analytical solution for the induced-stresses around circular hole in an elastic plate.

In this formulation, σ_x and σ_y are the in situ horizontal stresses (pre-mining stresses), σ_θ, σ_r, and $\tau_{r\theta}$ are the mining-induced stresses, a is the excavation radius, r is the distance to the interest point, and θ is the angle to the interest point measured counterclockwise from the horizontal axis.

When $a = r$, then σ_r and $\tau_{r\theta}$ are null and the induced-stress σ_θ at the wall of the excavation can be calculated as follows.

$$\sigma_\theta = \frac{(\sigma_x + \sigma_y)}{2} * \left(1 + \left(\frac{a}{r}\right)^2\right) - \frac{(\sigma_x - \sigma_y)}{2} * \left(1 + 4 * \left(\frac{a}{r}\right)^4\right) * \cos(2\theta)$$

An estimation of the effect of mining-induced stresses based on the spatial distribution of global rock mass strength-to-stress ratio was performed. The global rock mass strength, σ_{cm}, is the unconfined compressive strength defined by a Mohr-Coulomb fit to the Hoek-Brown curve over a range of confinement from 0 to 25% of the laboratory intact UCS. As a first approximation, the σ_{cm} strengths listed in Table 2 were used to estimate the adjustment factor given by the ratio $\sigma_\theta/\sigma_{cm}$, as shown in Figure 11.

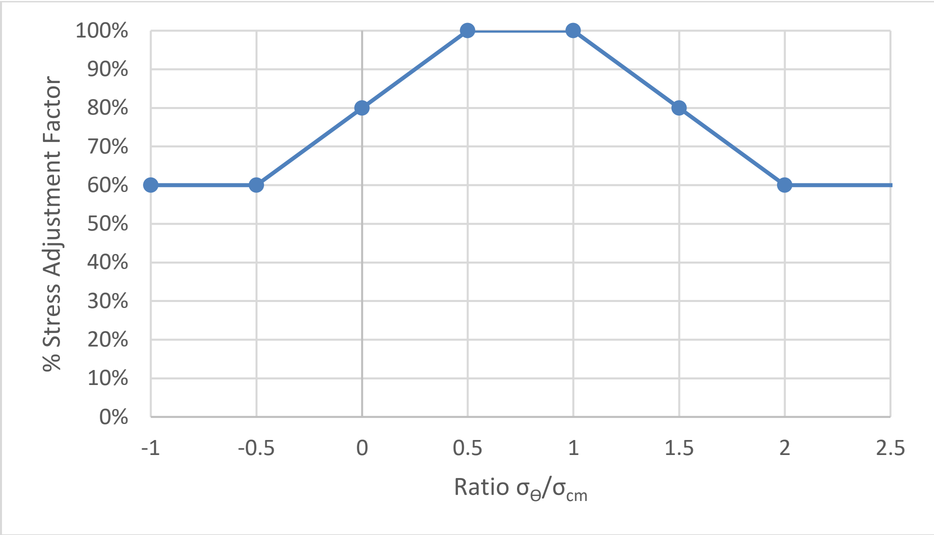

Figure 11 Adjustment Factor given by the ratio $\sigma_\theta/\sigma_{cm}$.

If the ratio $\sigma_\theta/\sigma_{cm}$ is between 0.5 and 1, the rock mass strength is enough to resist the hoop stresses around the cave; therefore, the adjustment factor will be 100% (MRMR=IRMR). On the other hand, if this ratio is greater than 1, the global rock mass strength would be less than the hoop stresses around the cave, which would indicate damage in the rock mass; therefore, the adjustment factor would go from 100% to 60% as the stress-to-strength ratio increases, leveling at 60% for stress-to-strength ratios larger than 2. Conversely, if this ratio is below 0.5, the lack of confinement could allow for joint opening; therefore, the adjustment factor would go from 100% to 60% as confinement is lost and would remain at 60% if in a more tensile environment.

This adjustment factor is calculated for each vertical subdivision (10 m height) marching upwards from the UCL to the ground surface.

5.0 RESULTS

The results of the Monte Carlo analyses are summarized in Table 4.

Table 4 Monte Carlo Results With Angle of Break Distributions Per Cross-Section Analyzed

Section	Graph	Min	Mean	Max	Std Dev	P20	P80
Section 1 WNW	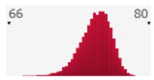	68	75	79	1	74	76
Section 1 ESE	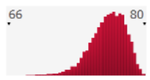	68	76	80	2	75	78
Section 2 NNW	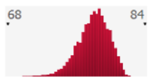	70	78	82	2	77	80
Section 2 SSE	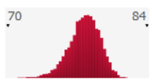	71	78	82	1	77	79
Section 3 SE	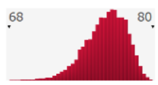	68	76	80	2	75	78
Section 3 NW	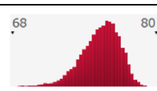	69	75	79	2	74	77
Section 4 SW	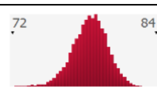	72	79	83	1	77	80
Section 4 NE	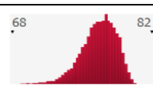	69	77	80	2	75	78
Section 5 SW	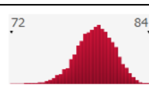	72	79	84	2	78	81
Section 5 NE	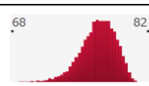	69	77	81	2	75	78
Section 6 SW	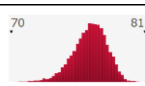	71	76	80	1	75	78
Section 6 NE	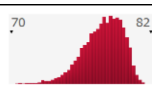	71	78	81	2	76	79
Section 7 NW	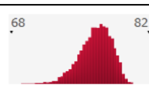	69	77	80	2	75	78
Section 7 SE	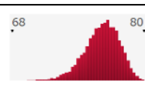	70	76	80	2	75	77

Using the Laubscher's method, the resulting angle of break (mean value) at Resolution Copper Mine varies between 74º and 79º, with a standard deviation around 2º.

This study suggests an average cave angle of 77º, which is in general agreement with the results of numerical analysis carried out by Garza-Cruz & Pierce (2017) predicting cave angles between 70 – 78°.

The detail of characterization by section can be found in Appendix 1. The resulting angle of break distributions can be found in Appendix 2.

6.0 CONCLUSIONS

A probabilistic approach to Laubscher's Method for subsidence prediction has been carried out at Resolution Copper to estimate cave angles resulting from panel caving. Monte Carlo simulations were conducted using @RISK to estimate a probabilistic distribution of angle of break on seven vertical cross-sections. The IRMR distributions per geotechnical domain were used to inform the Monte Carlo sampling.

Given the available IRMR database, a MRMR adjustment procedure was carried out to incorporate mining-induced stresses given by the Kirsch analytical solution and the rock mass strength.

The results for the seven sections under study indicate an average angle of break between 74º and 79º, with an overall average of 77º. This is in general agreement with the results of previous numerical analysis performed by Garza-Cruz & Pierce (2017).

Although Laubscher's method is based on limited data, it can be a useful approach to capture tendencies and to obtain an initial understanding of subsidence resulting from caving.

7.0 REFERENCES

Garza-Cruz T. & M. Pierce (2017) "Assessment of Surface Subsidence Associated with Caving Resolution Copper Mine Plan of Operations", Itasca Consulting Group, Inc., Technical Report to Resolution Copper Company.

Laubscher D. (2000) "Block Caving Manual". Report for the international caving study. JKMRC and Itasca Consulting Group, Brisbane.

Laubscher, D. H., and J. Jakubec. (2001) "The MRMR Rock Mass Classification for Jointed Rock Mass," in ***Underground Mining Methods: Engineering Fundamentals and International Case Studies***. Englewood, Colorado: SME.

van As A, Davison J & Moss A. (2003) "Subsidence definitions for block caving mines". Rio Tinto technical services.

8.0 APPENDIX 1

This section contains a general description of the seven cross-sections analyzed (see Figure 8).

8.1 Section 1

Figure 12 shows the geotechnical domains and resulting cave angles across Section 1. Table 5 and Table 6 shown the geotechnical characterization detail across this section.

This section has a minimum span of 1440 meters with angles (θ in Kirsch analytical solution) of 170.5 and -9.5 degrees (counterclockwise from the East) for WNW and ESE, respectively.

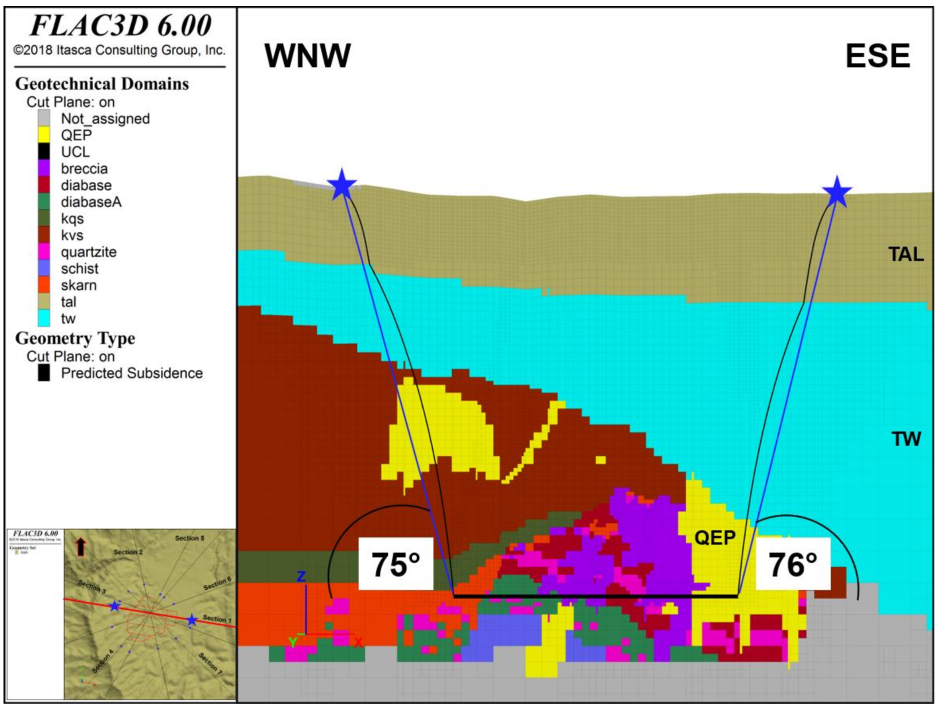

Figure 12 Geotechnical domains and resulting cave angles across Section 1.

Table 5 Characterization of Section 1 WNW.

Division	Thickness [m]	Geotechnical Domain
H1_WNW	40	Skarn
H2_WNW	140	KQS
H3_WNW	1040	KVS
H4_WNW	450	TW
H5_WNW	390	TAL
Total	2060	-

Table 6 Characterization of Section 1 ESE.

Division	Thickness [m]	Geotechnical Domain
H1_ESE	300	QEP
H2_ESE	1170	TW
H3_ESE	550	TAL
Total	2060	-

8.2 Section 2

Figure 13 shows the geotechnical domains and resulting cave angles across Section 2. Table 7 and Table 8 shown the geotechnical characterization detail across this section.

This section has a minimum span of 1250 meters with angles (θ in Kirsch analytical solution) of 102.2 and 77.8 degrees (counterclockwise from the East) for NNW and SSE, respectively.

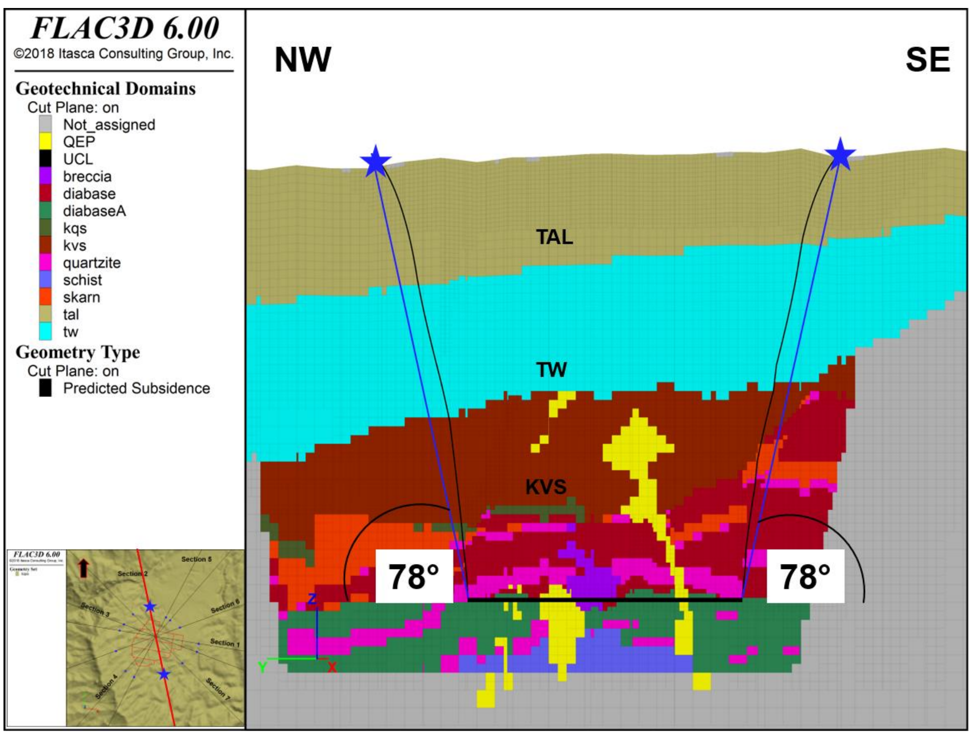

Figure 13 Geotechnical domains and resulting cave angles across Section 2.

Table 7 Characterization of Section 2 NNW.

Division	Thickness [m]	Geotechnical Domain
H1_NNW	70	Quartzite
H2_NNW	160	Diabase
H3_NNW	120	Skarn
H4_NNW	445	KVS
H5_NNW	650	TW
H6_NNW	575	TAL
Total	2020	-

Table 8 Characterization of Section 2 SSE.

Division	Thickness [m]	Geotechnical Domain
H1_SSE	140	Diabase
H2_SSE	80	Quartzite
H3_SSE	280	Diabase
H4_SSE	120	Skarn
H5_SSE	320	Diabase
H6_SSE	120	KVS
H7_SSE	580	TW
H8_SSE	380	TAL
Total	2020	-

8.3 Section 3

Figure 14 shows the geotechnical domains and resulting cave angles across Section 3. Table 9 and Table 10 shown the geotechnical characterization detail across this section.

This section has a minimum span of 1350 meters with angles (θ in Kirsch analytical solution) of 159 and -21 degrees (counterclockwise from the East) for NW and SE, respectively.

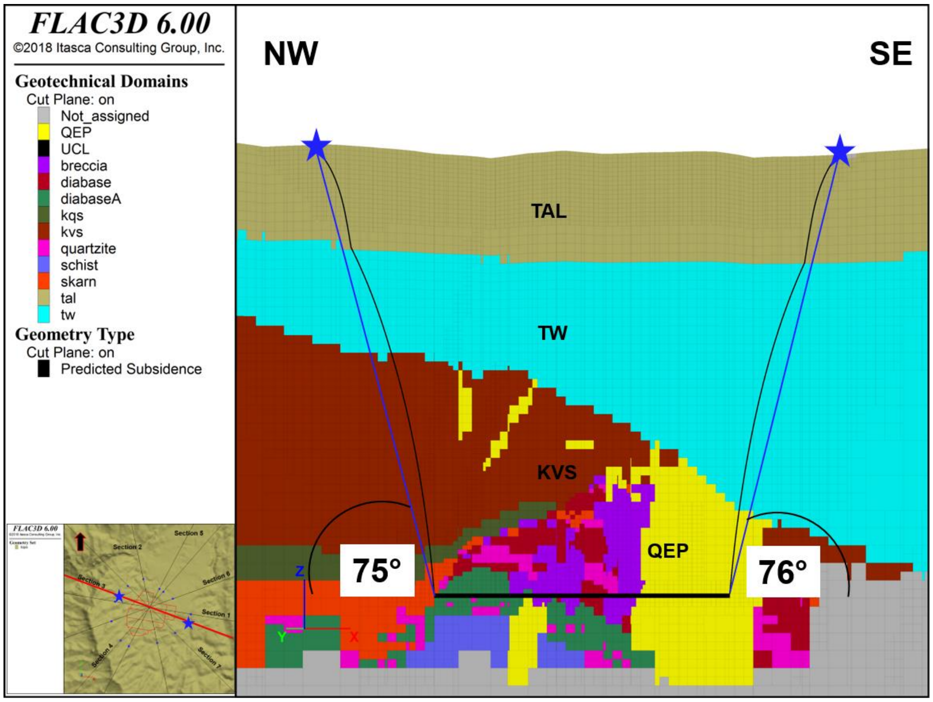

Figure 14 Geotechnical domains and resulting cave angles across Section 3.

Table 9 Characterization of Section 3 NW.

Division	Thickness [m]	Geotechnical Domain
H1_NW	120	Skarn
H2_NW	80	KQS
H3_NW	920	KVS
H4_NW	460	TW
H5_NW	440	TAL
Total	2020	-

Table 10 Characterization of Section 3 SE.

Division	Thickness [m]	Geotechnical Domain
H1_SE	380	QEP
H2_SE	1130	TW
H3_SE	500	TAL
Total	2010	-

8.4 Section 4

Figure 15 shows the geotechnical domains and resulting cave angles across Section 4. Table 11 and Table 12 shown the geotechnical characterization detail across this section.

This section has a minimum span of 1200 meters with angles (θ in Kirsch analytical solution) of -131 and 49 degrees (counterclockwise from the East) for SW and NE, respectively.

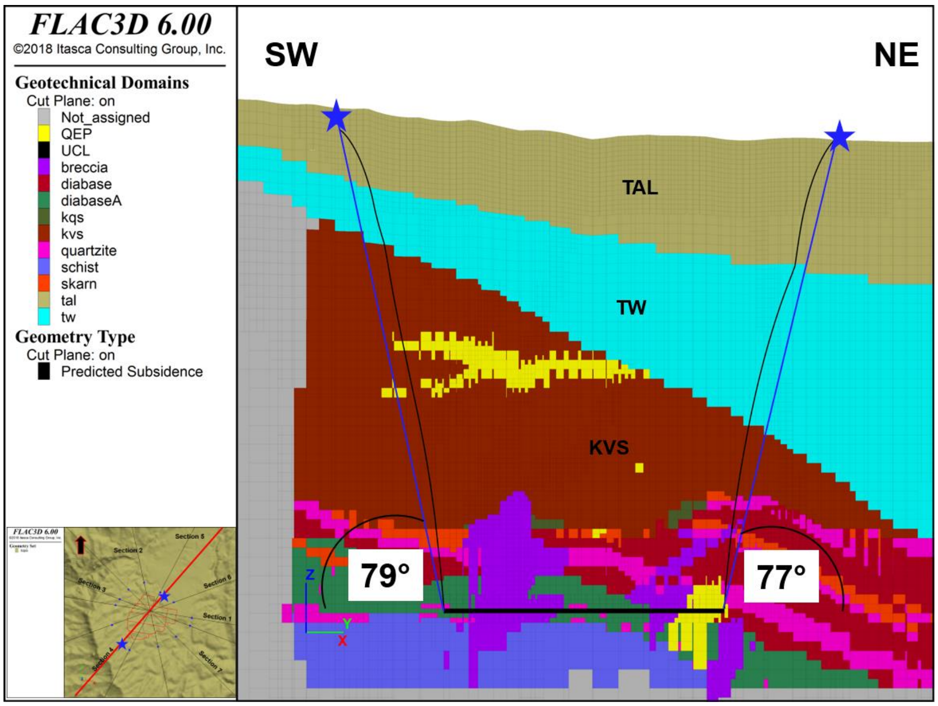

Figure 15 Geotechnical domains and resulting cave angles across Section 4.

Table 11 Characterization of Section 4 SW.

Division	Thickness [m]	Geotechnical Domain
H1_SW	130	DiabaseA
H2_SW	140	Diabase
H3_SW	120	Skarn
H4_SW	1170	KVS
H5_SW	190	TW
H6_SW	290	TAL
Total	2040	-

Table 12 Characterization of Section 4 NE.

Division	Thickness [m]	Geotechnical Domain
H1_NE	100	Quartzite
H2_NE	120	Diabase
H3_NE	80	Skarn
H4_NE	160	Diabase
H5_NE	240	KVS
H6_NE	760	TW
H7_NE	550	TAL
Total	2010	-

8.5 Section 5

Figure 16 shows the geotechnical domains and resulting cave angles across Section 5. Table 13 and Table 14 shown the geotechnical characterization detail across this section.

This section has a minimum span of 1207 meters with angles (θ in Kirsch analytical solution) of -118 and 62 degrees (counterclockwise from the East) for SW and NE, respectively.

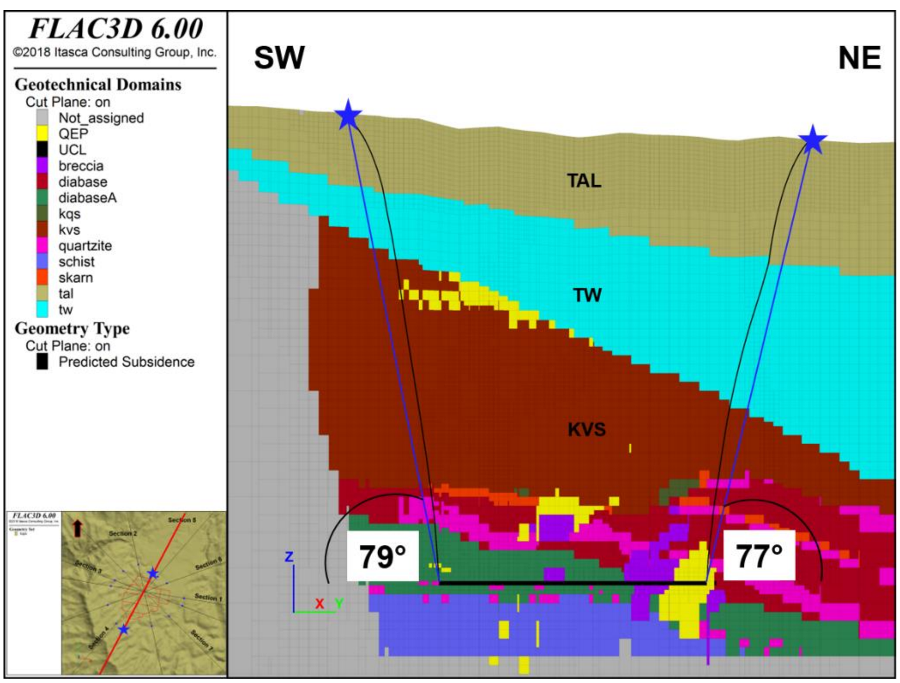

Figure 16 Geotechnical domains and resulting cave angles across Section 5.

Table 13 Characterization of Section 5 SW.

Division	Thickness [m]	Geotechnical Domain
H1_SW	260	DiabaseA
H2_SW	160	Diabase
H3_SW	1200	KVS
H4_SW	160	TW
H5_SW	300	TAL
Total	2080	-

Table 14 Characterization of Section 5 NE.

Division	Thickness [m]	Geotechnical Domain
H1_NE	40	Diabase
H2_NE	60	Quartzite
H3_NE	160	Diabase
H4_NE	60	Skarn
H5_NE	150	Diabase
H6_NE	230	KVS
H7_NE	740	TW
H7_NE	560	TAL
Total	2000	-

8.6 Section 6

Figure 17 shows the geotechnical domains and resulting cave angles across Section 6. Table 15 and Table 16 shown the geotechnical characterization detail across this section.

This section has a minimum span of 1130 meters with angles (θ in Kirsch) of -160 and 20 degrees (counterclockwise from the East) for SW and NE, respectively.

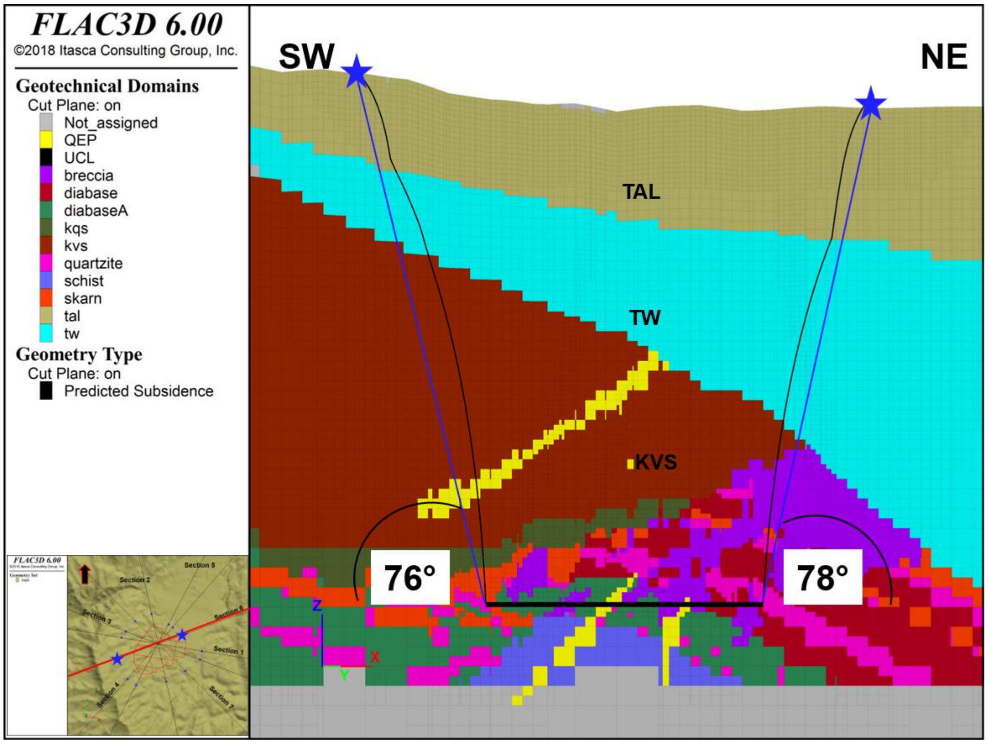

Figure 17 Geotechnical domains and resulting cave angles across Section 6.

Table 15 Characterization of Section 6 SW.

Division	Thickness [m]	Geotechnical Domain
H1_SW	150	Skarn
H2_SW	100	KQS
H3_SW	120	KVS
H4_SW	110	QEP
H5_SW	1040	KVS
H6_SW	280	TW
H7_SW	350	TAL
Total	2150	-

Table 16 Characterization of Section 6 NE.

Division	Thickness [m]	Geotechnical Domain
H1_NE	70	Quartzite
H2_NE	490	Breccia
H3_NE	920	TW
H4_NE	580	TAL
Total	2060	-

8.7 Section 7

Figure 18 shows the geotechnical domains and resulting cave angles across Section 7. Table 17 and Table 18 shown the geotechnical characterization detail across this section.

This section has a minimum span of 1160 meters with angles (θ in Kirsch analytical solution) of 135 and -45 degrees (counterclockwise from the East) for NW and SE, respectively.

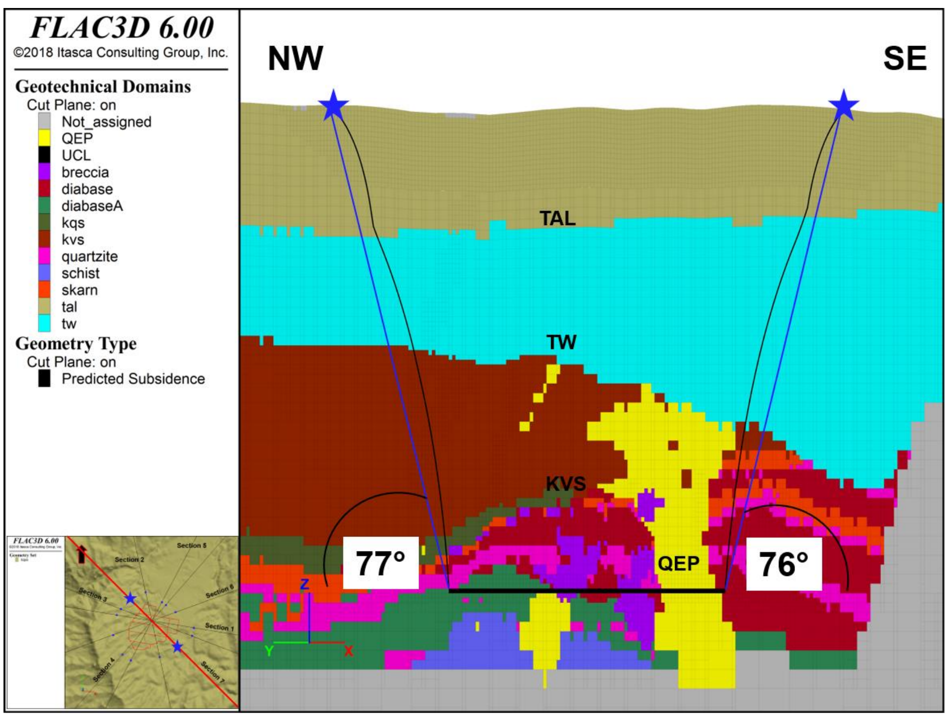

Figure 18 Geotechnical domains and resulting cave angles across Section 7.

Table 17 Characterization of Section 7 NW.

Division	Thickness [m]	Geotechnical Domain
H1_NW	100	Quartzite
H2_NW	80	KQS
H3_NW	840	KVS
H4_NW	500	TW
H5_NW	490	TAL
Total	2010	-

Table 18 Characterization of Section 7 SE.

Division	Thickness [m]	Geotechnical Domain
H1_SE	80	Diabase
H2_SE	40	Quartzite
H3_SE	180	Diabase
H4_SE	90	Skarn
H5_SE	100	Diabase
H6_SE	1110	TW
H7_SE	410	TAL
Total	2010	-

9.0 APPENDIX 2

This section contains the resulting distribution of angle of break per cross section analyzed.

9.1 Section 1

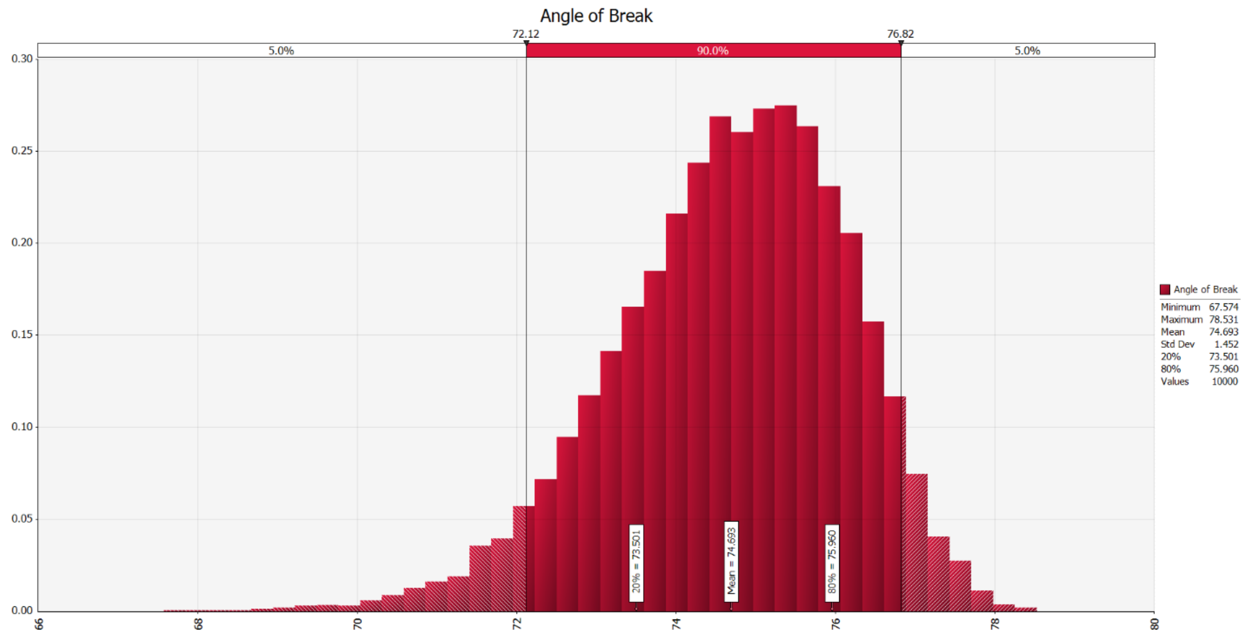

Figure 19 Probabilistic distribution of angle of break across Section 1 WNW.

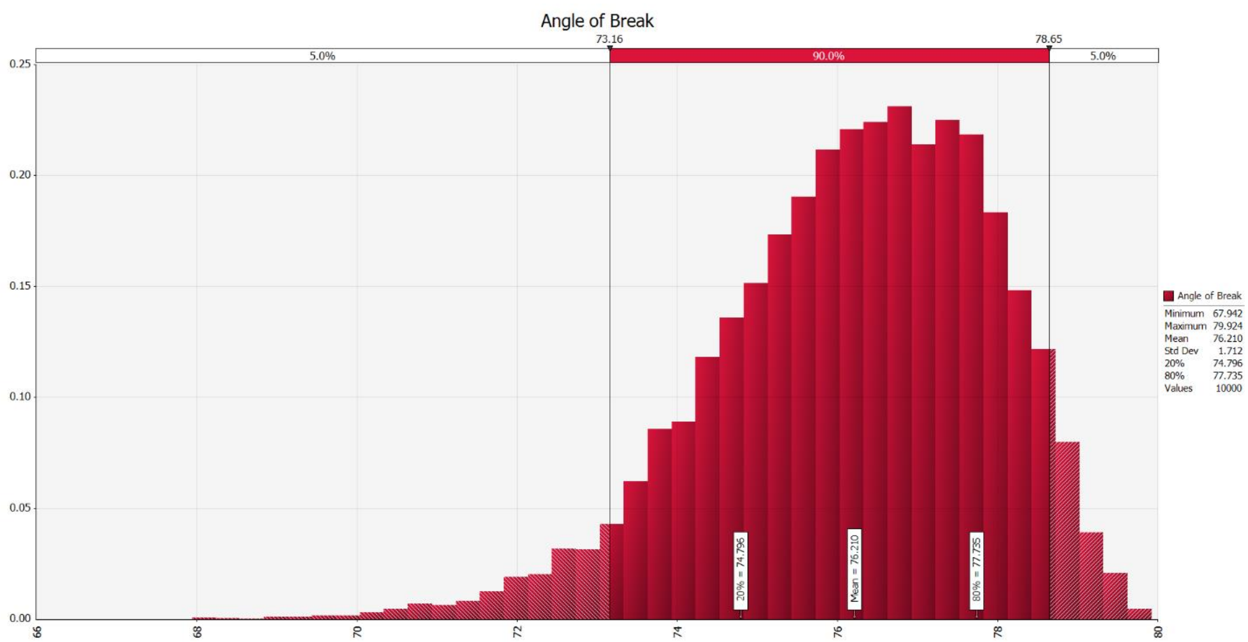

Figure 20 Probabilistic distribution of angle of break across Section 1 ESE.

9.2 Section 2

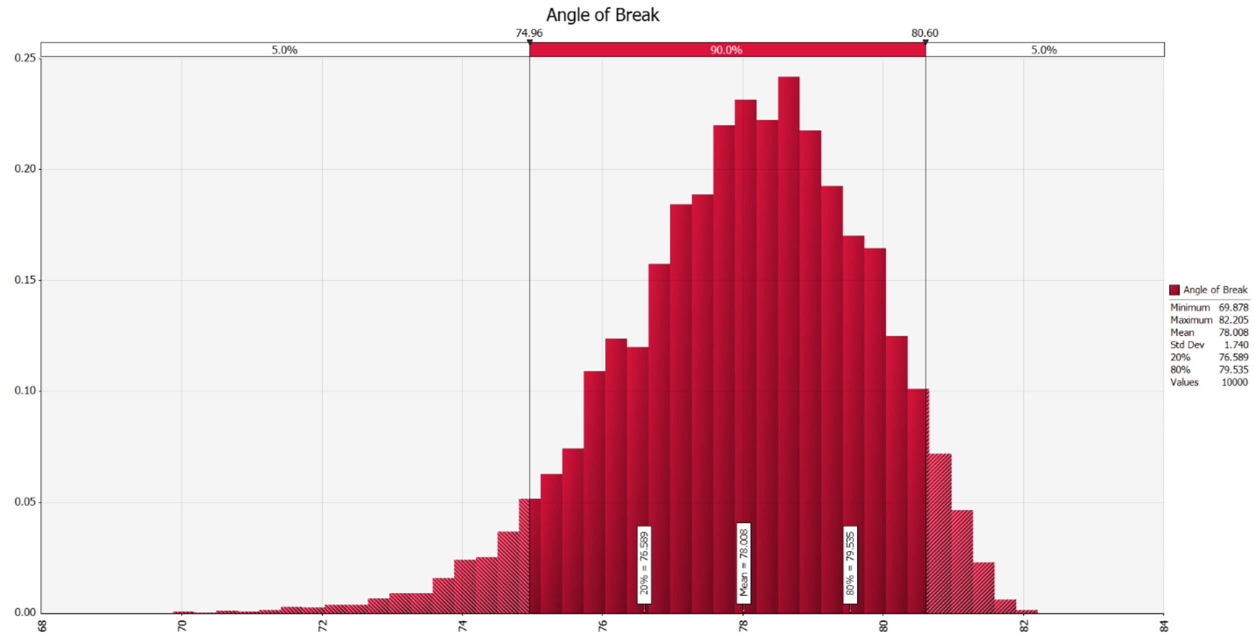

Figure 21 Probabilistic distribution of angle of break across Section 2 NNW.

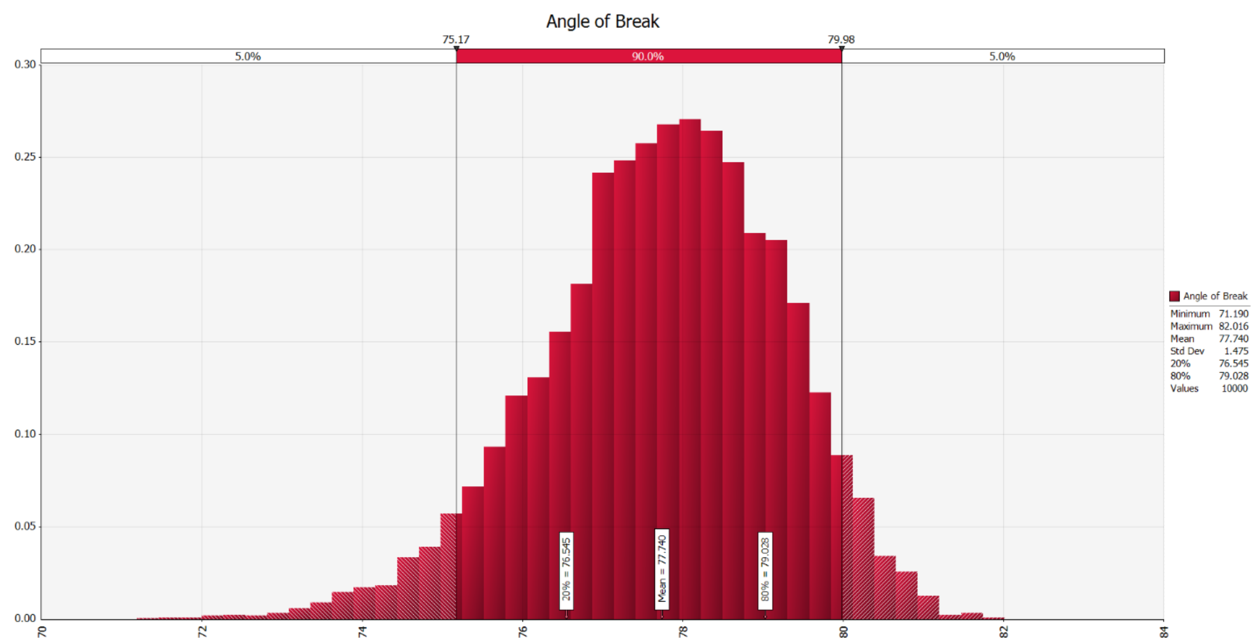

Figure 22 Probabilistic distribution of angle of break across Section 2 SSE.

9.3 Section 3

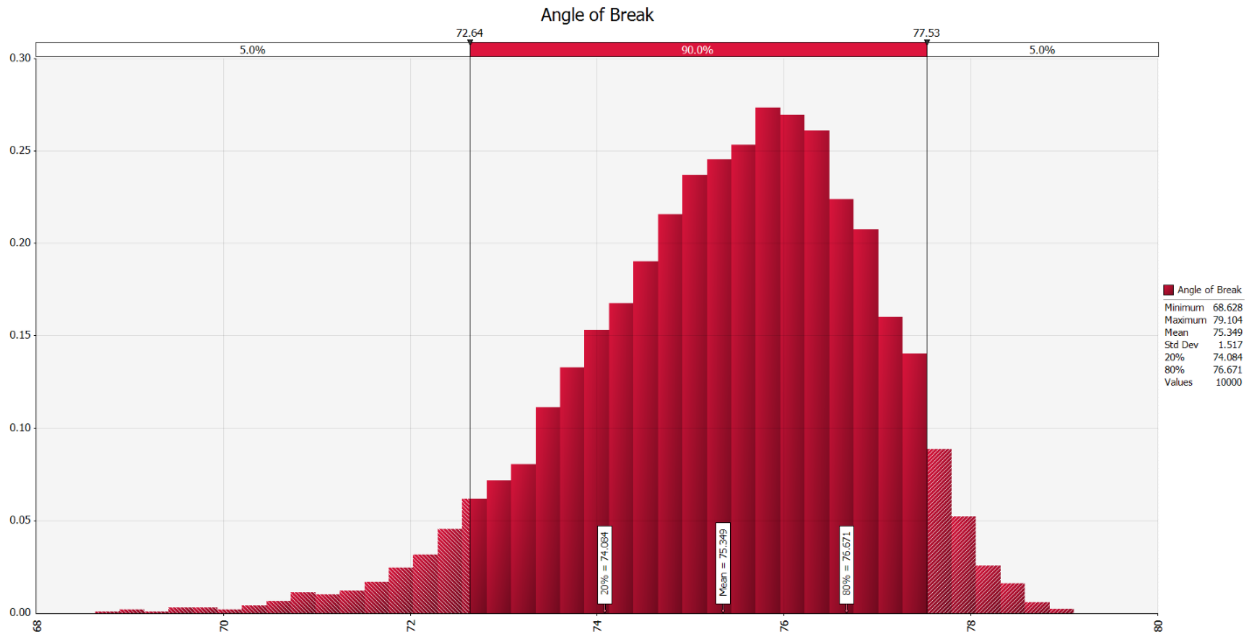

Figure 23 Probabilistic distribution of angle of break across Section 3 NW.

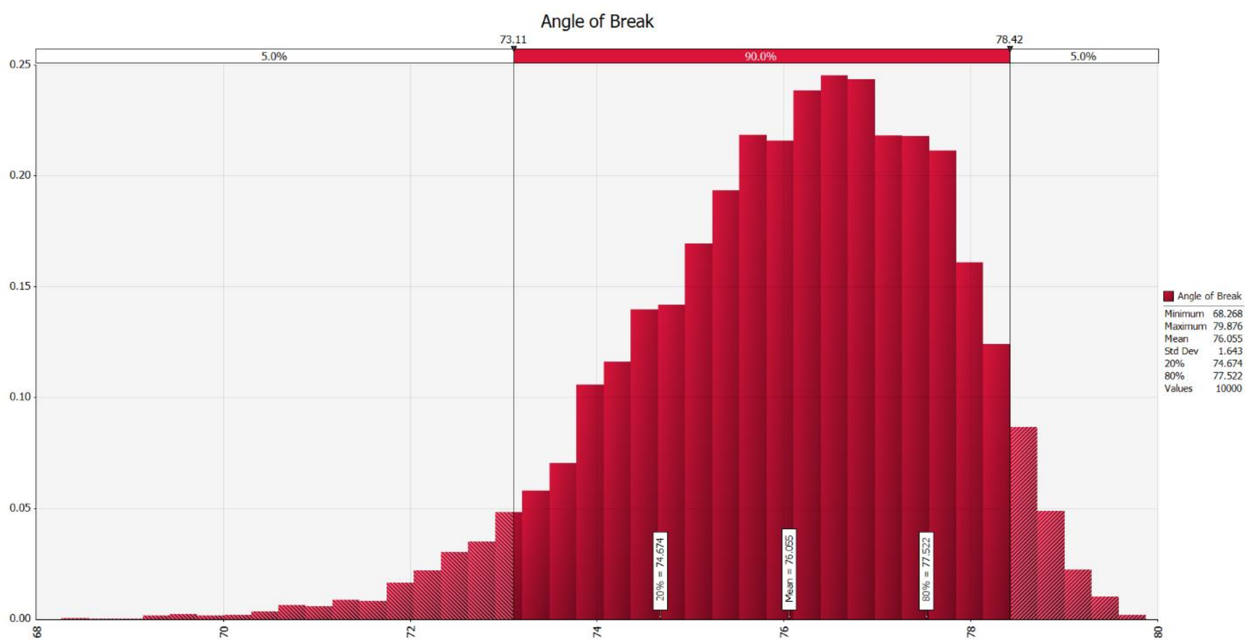

Figure 24 Probabilistic distribution of angle of break across Section 3 SE.

9.4 Section 4

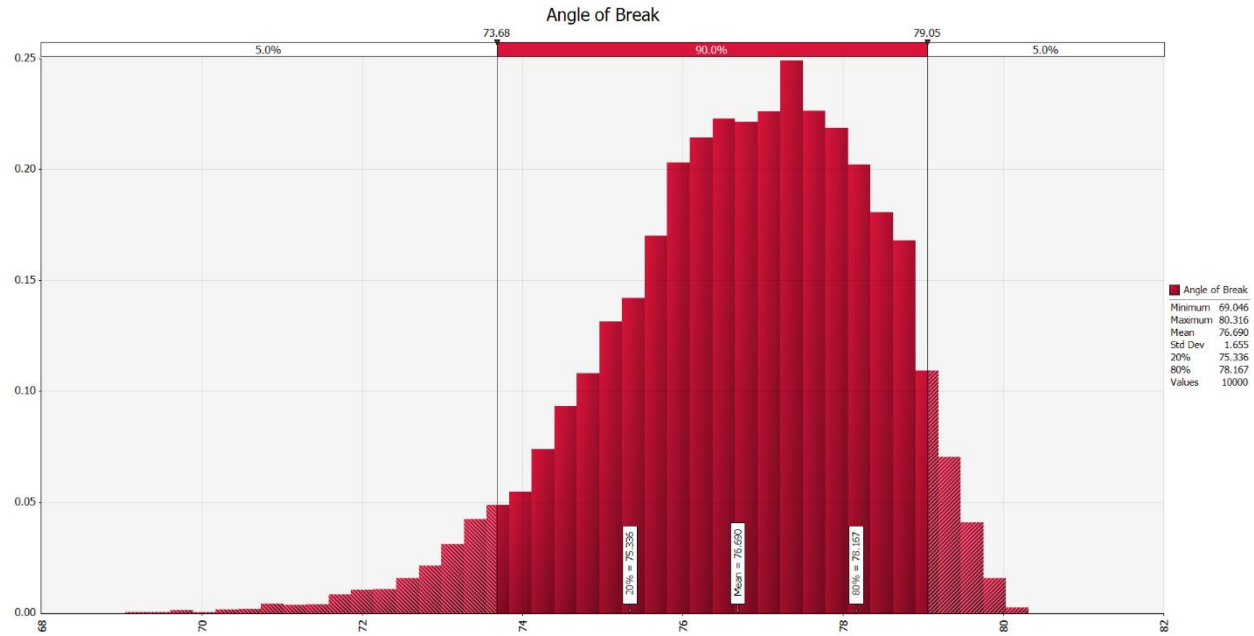

Figure 25 Probabilistic distribution of angle of break across Section 4 NE.

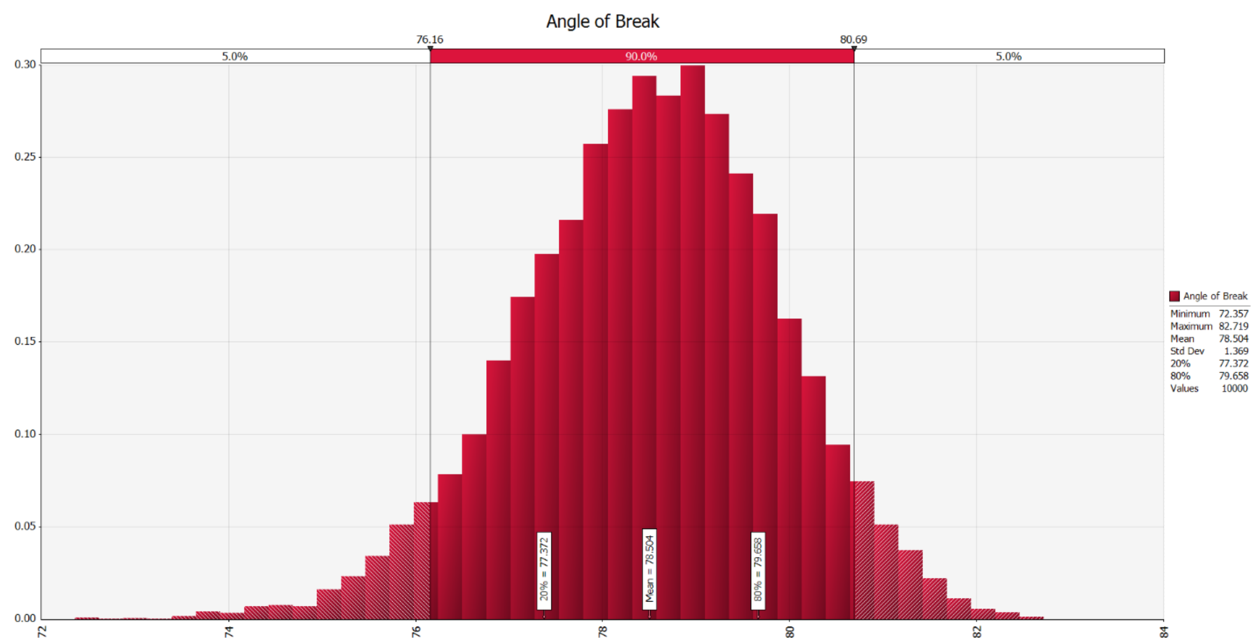

Figure 26 Probabilistic distribution of angle of break across Section 4 SW.

9.5 Section 5

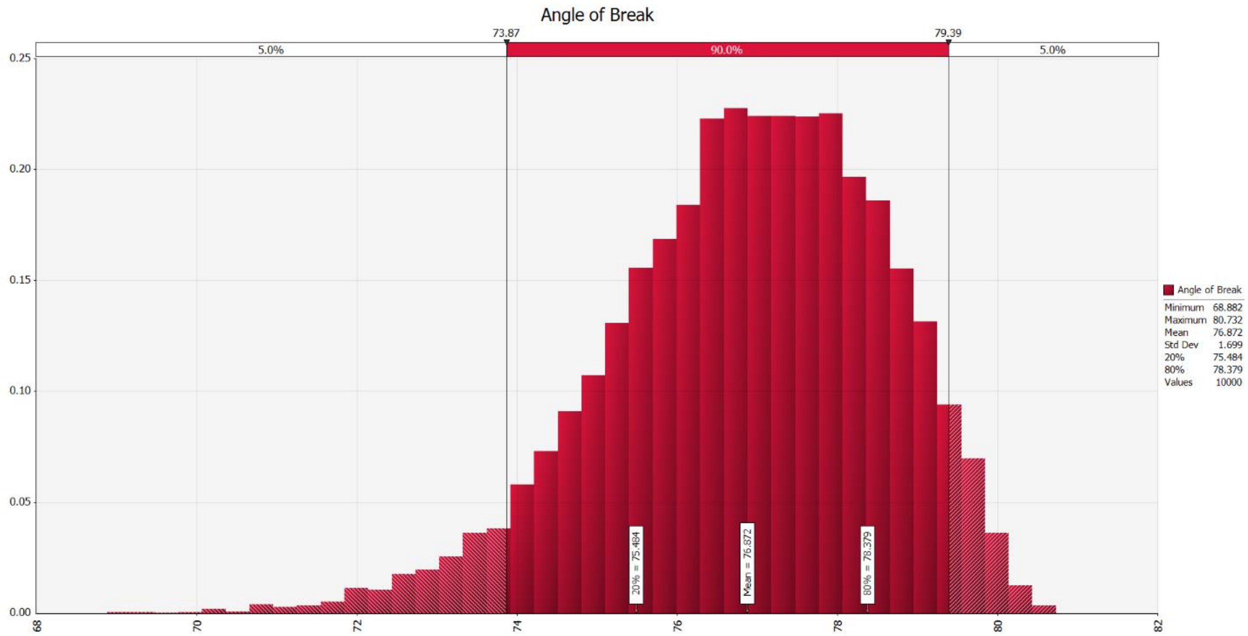

Figure 27 Probabilistic distribution of angle of break across Section 5 NE.

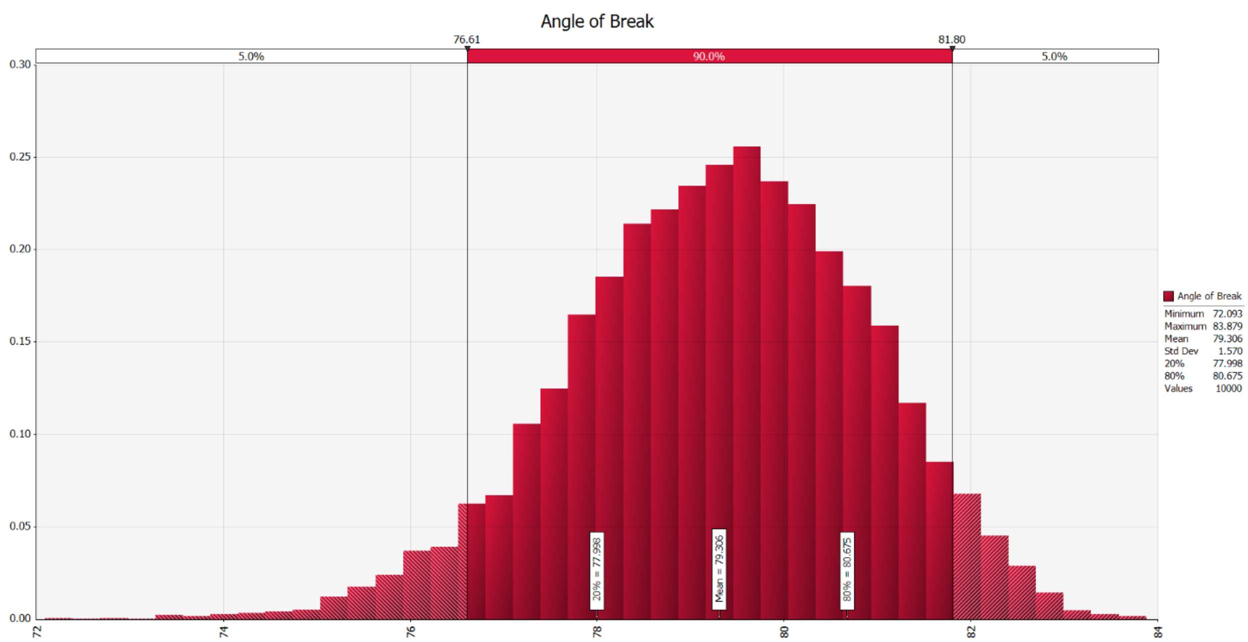

Figure 28 Probabilistic distribution of angle of break across Section 5 SW.

9.6 Section 6

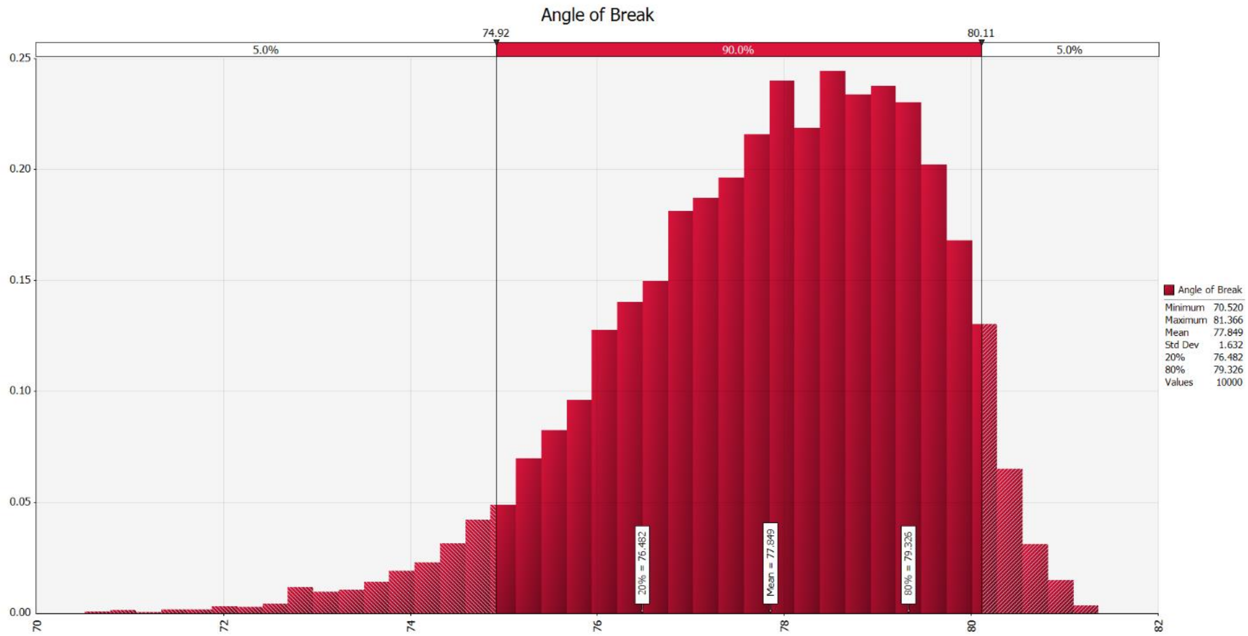

Figure 29 Probabilistic distribution of angle of break across Section 6 NE.

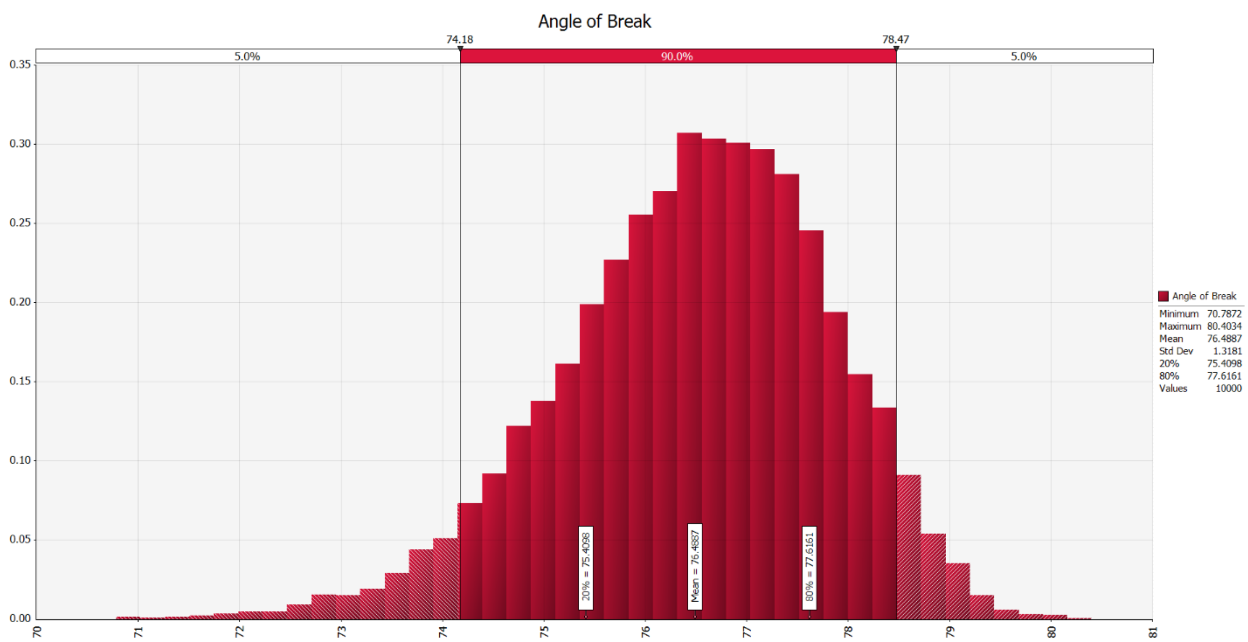

Figure 30 Probabilistic distribution of angle of break across Section 6 SW.

9.7 Section 7

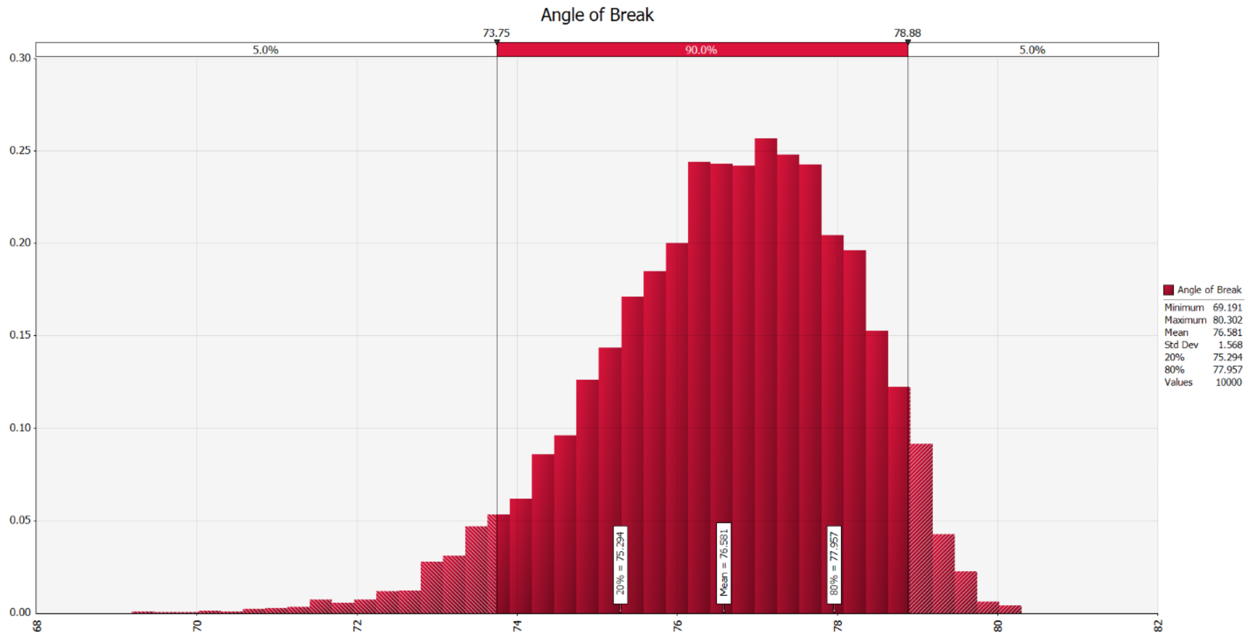

Figure 31 Probabilistic distribution of angle of break across Section 7 NW.

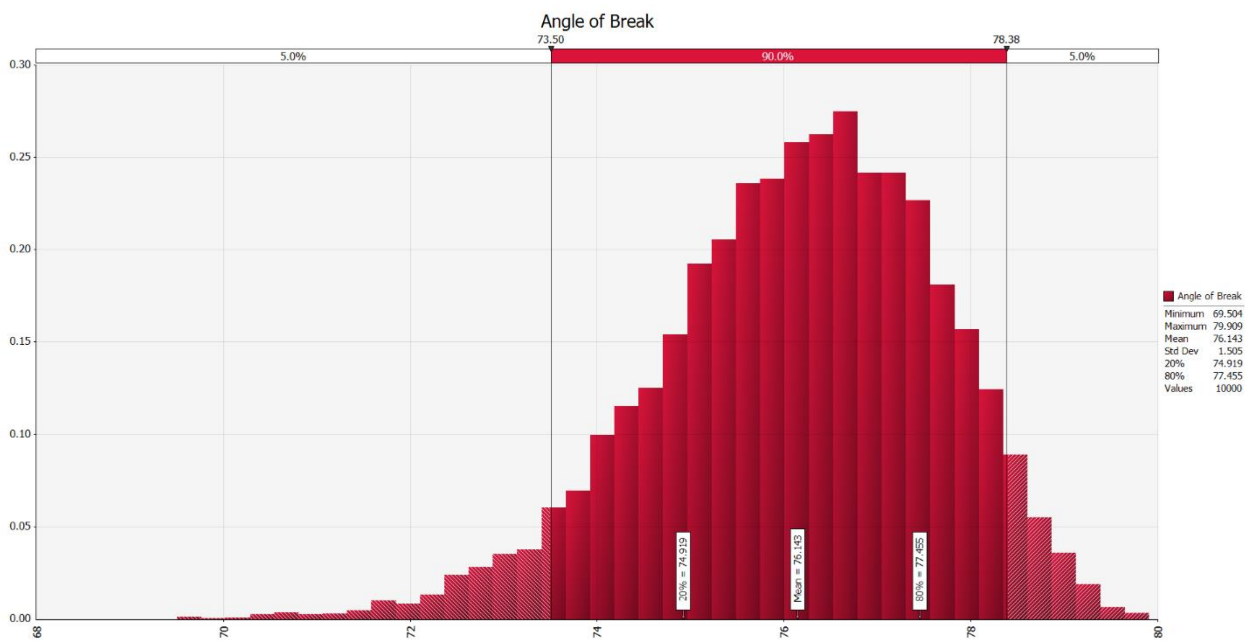

Figure 32 Probabilistic distribution of angle of break across Section 7 SE.

Victoria Boyne

Subject: FW: EXTERNAL:Response to Data Request - Geology/Subsidence - Empirical Subsidence Analysis
Attachments: 2-4208-04_19R32_EmpiricalSubsidence.pdf

From: Peacey, Victoria (RC) <Victoria.Peacey@riotinto.com>
Sent: Thursday, May 16, 2019 12:24 PM
To: Rasmussen, Mary C -FS (mary.rasmussen@usda.gov) <mary.rasmussen@usda.gov>
Cc: Donna Morey <dmorey@swca.com>; Chris Garrett <cgarrett@swca.com>; RCPermitting <RCPermitting@riotinto.com>
Subject: EXTERNAL:Response to Data Request - Geology/Subsidence - Empirical Subsidence Analysis

Hello Mary,

For your review and consideration and in response to the Geology/Subsidence Data Request, please see the Empirical Subsidence Analysis Technical report by Itasca.

Thanks,

Vicky Peacey
Senior Manager – Permitting and Approvals

RESOLUTION
COPPER
102 Magma Heights
Superior, AZ 85173, United States
T: +1 520.689.3313 M: +1 520.827.1136
victoria.peacey@riotinto.com www.resolutioncopper.com